Applied Catalysis B: Environmental 165 (2015) 589–598

Contents lists available at ScienceDirect

Applied Catalysis B: Environmental

journal homepage: www.elsevier.com/locate/apcatb

Getting insight into the influence of SO_2 on TiO_2/CeO_2 for the selective catalytic reduction of NO by NH_3

Lei Zhang[a,b], Lulu Li[a,b], Yuan Cao[a,b], Xiaojiang Yao[a,b], Chengyan Ge[a,b], Fei Gao[a,b,*], Yu Deng[b], Changjin Tang[a,b], Lin Dong[a,b,*]

[a] Key Laboratory of Mesoscopic Chemistry of MOE, School of Chemistry and Chemical Engineering, Nanjing University, Nanjing 210093, PR China
[b] Jiangsu Key Laboratory of Vehicle Emissions Control, Center of Modern Analysis, Nanjing University, Nanjing 210093, PR China

ARTICLE INFO

Article history:
Received 21 July 2014
Received in revised form
19 September 2014
Accepted 10 October 2014
Available online 22 October 2014

Keywords:
NH_3-SCR
TiO_2/CeO_2
SO_2 resistance
in situ DRIFT
Sulfates

ABSTRACT

A series of inverse TiO_2/CeO_2 catalysts were prepared by the impregnation method and their catalytic performances for the selective catalytic reduction of NO by NH_3 have been tested with and without SO_2 and/or H_2O. Compared with the normally discussed CeO_2/TiO_2 catalyst, the advantage of inverse TiO_2/CeO_2 catalyst was not only shown a good low temperature catalytic activity (150–250 °C), but also exhibited much better SO_2 resistance performances with the existence of 200 ppm SO_2 and/or 5 vol.% H_2O at 300 °C. Furthermore, SO_2 had more significant inhibitory effect on catalytic activity than H_2O based on the configuration differences of Ce–Ti-based catalysts. These catalysts were investigated by means of TG-DTA, XRD, BET, *in situ* DRIFT, XPS and H_2-TPR. The results demonstrated that the sulfation of these samples under reactive conditions mainly generated three different kinds of sulfate species including NH_4HSO_4, surface and bulk-like metal sulfates (mainly interacted with cerium species). The formed metal sulfates blocked the active sites of Ce–O–Ti and resulted in the deactivation of CeO_2/TiO_2. Although metal sulfates were also formed over TiO_2/CeO_2, NH_3-SCR could still proceed and that was similar as the reaction system with the use of sulfated CeO_2 as the catalyst. Meanwhile, the interactions between SO_2 and Ce–Ti-based catalysts were discussed in detail and an adsorption model of SO_2 was proposed.

1. Introduction

Nitrogen oxides (NO_x) have caused a series of atmospheric pollution problems such as acid rain, photochemical smog and ozone depletion. Generally, NO_x emissions are produced from stationary or mobile sources, including coal-fired power plants and vehicle engines. Selective catalytic reduction of NO_x by NH_3 (NH_3-SCR) technique has been demonstrated as an effective NO_x removal approach for stationary source. In this area, V_2O_5–WO_3/TiO_2 is the most widely used commercial NH_3-SCR catalyst due to high deNO_x efficiency in the range of 300–400 °C and excellent resistance to SO_2 poisoning. However, this type of catalyst also has significant drawbacks, such as over-oxidation of NH_3 to N_2O or NO at high temperature and the toxicity of vanadium [1–5]. To search for a suitable replacement of V_2O_5–WO_3/TiO_2 catalyst, some new environmentally benign catalysts with evaluated NH_3-SCR activity have been extensively studied. For example, Cu- and Fe-exchanged zeolite catalysts exhibited good activities in a wide temperature range [4,6–8]. Other nontoxic transition metal oxide-based catalysts such as CeO_2–TiO_2-based catalysts [9,10], FeO_x–TiO_2-based catalysts [11–14] and CeO_2–WO_x-based catalysts [15,16] have also been investigated as potential alternatives.

Herein, we focus on the development of Ce–Ti-based catalysts for NH_3-SCR. Experimental results suggest that optimized Ce–Ti-based catalysts exhibit excellent NO_x removal rate and N_2 selectivity at mediate-high temperature [17,18]. It is reported that CeO_2/TiO_2 catalyst prepared by traditional impregnation method had poor SO_2 resistance, which limited its practical application [19]. One way to improve the SO_2 resistance of CeO_2–TiO_2 catalyst is adding modification agents to CeO_2–TiO_2 catalyst. As reported by Shan et al. [20], with the addition of WO_3 into CeO_2–TiO_2 to form $Ce_{0.2}W_{0.2}TiO_x$, NO_x conversion was maintained at nearly 100% for 12 h in the presence of 100 ppm SO_2 at 300 °C. Shen et al. [21] found similar promotion effect of a zirconium additive on the catalytic performance of $Ti_{0.8}Ce_{0.2}O_2$. Liu et al. [22] reported that Ce/TiO_2–SiO_2 exhibited superior strong resistance to SO_2 than Ce/TiO_2, and their study suggested that the introduction of SiO_2 further weakened the alkalinity over the surface of

* Corresponding authors. Tel.: +86 25 83592290; fax: +86 25 83317761.
E-mail addresses: gaofei@nju.edu.cn (F. Gao), donglin@nju.edu.cn (L. Dong).

http://dx.doi.org/10.1016/j.apcatb.2014.10.029
0926-3373/

Ce/TiO_2–SiO_2, which decreased the accumulation of sulfate on the surface of Ce/TiO_2–SiO_2 compared with Ce/TiO_2. Another reported route is to improve the preparation method of CeO_2–TiO_2 catalyst. For example, Gao et al. [23] reported that samples prepared by sol–gel method displayed better SO_2 resistance than samples prepared by impregnation and co-precipitation method. Moreover, Shan et al. [18] reported that NO conversion almost had no change by addition of 100 ppm SO_2 for 24 h at 300 °C over Ce–Ti mixed oxide prepared by homogeneous precipitation method. Although some progresses have been made in improving SO_2 resistance of Ce–Ti-based catalysts, more detailed studies are needed to understand the interaction mechanism between SO_2 and Ce–Ti-based catalysts during NH_3-SCR process.

In the present work, we report a novel strategy to obtain TiO_2/CeO_2 with enhanced SO_2 resistance by simply modifying the configuration of CeO_2/TiO_2. We find that NO conversion of TiO_2/CeO_2 could be constantly maintained at *ca.* 90% in the process of 25 h test with 200 ppm SO_2 at 300 °C. However, NO conversion gradually decreased to about 46% under the same conditions for CeO_2/TiO_2. CeO_2, TiO_2/CeO_2 and CeO_2/TiO_2 samples were characterized by TG-DTA, XRD, BET, *in situ* DRIFT, XPS and H_2-TPR in order to illustrate the influence of configuration on SO_2 resistance. And then, we proposed the SO_2 resistance models of Ce–Ti-based catalysts for NH_3-SCR. Finally, we hope that this work will guide us to design the high performance Ce–Ti-based catalysts with excellent SO_2 resistance for NH_3-SCR.

2. Experimental

2.1. Sample preparation

CeO_2 was prepared by thermal decomposition of $Ce(NO_3)_3 \cdot 6H_2O$ at 550 °C for 4 h in flowing air. TiO_2 support was prepared by $TiCl_4$-dropwise into ethanol–water solution in an ice–water bath under stirring, after that adding appropriate amount of $NH_3 \cdot H_2O$ into the solution until the pH value was 9.0. The precipitate was washed with distilled water until no chloride ions which were detected by $AgNO_3$ solution, then dried at 110 °C for 12 h and calcined at 500 °C for 4 h in flowing air.

TiO_2/CeO_2 and CeO_2/TiO_2 samples were prepared by incipient wetness impregnation. For TiO_2/CeO_2 samples, the requisite quantity of tetrabutyl titanate dropped into ethanol in an ice–water bath under stirring then adding appropriate amount of CeO_2 to the mixture solution. After that, proper amount of water was added. The solvent was evaporated at 100 °C, and then dried at 120 °C for 3 h, calcined at 500 °C for 4 h in flowing air. For CeO_2/TiO_2, TiO_2 was added to the solution of $Ce(NO_3)_3 \cdot 6H_2O$ under stirring, then evaporated at 100 °C until achieving a paste, which was dried at 110 °C overnight and calcined in a muffle stove at 500 °C for 4 h in flowing air. For simplify, TiO_2/CeO_2 samples were shorted for Ti_x/Ce_y, where x and y were the molar ratio of TiO_2 to CeO_2. CeO_2/TiO_2 was denoted as Ce/Ti and the molar ratio of Ce/Ti was fixed at 1:20. Furthermore, CeO_2 and TiO_2 were mechanically mixed with the molar ratio of TiO_2 to CeO_2 was 2:8 (denoted as TiCe mixture). Taking Ce/Ti as an example, the used sample tested in the presence of SO_2 for 25 h was shorted for Ce/Ti-U.

2.2. Characterization

Thermogravimetry and differential thermal analysis (TG-DTA) of the samples was carried out on a Netzsch thermoanalyzer STA 449C with a heating rate of 5 °C min^{-1} in a flowing air.

X-ray powder diffraction (XRD) patterns were collected using a Philips X'pert Pro diffractometer with Ni-filtered Cu Kα1 radiation (0.15408 nm). The X-ray tube was operated at 40 kV and 40 mA.

Specific surface areas of samples were measured by nitrogen adsorption at 77 K on a Micrometrics ASAP-2020 analyzer by the Brunauer–Emmet–Teller (BET) method. Before each adsorption measurement, about 0.1 g catalyst sample was degassed in a N_2/He mixture at 300 °C for 4 h.

H_2-TPR was carried out in a quartz U-tube reactor connected to a TCD with H_2–Ar mixture (7% H_2 by volume) as reductant. Fifty milligrams of sample were used for each measurement. Before switching to the H_2–Ar stream, the sample was pretreated in a N_2 stream at 200 °C for 1 h. TPR started from room temperature to 850 °C at a rate of 10 °C min^{-1}.

X-ray photoelectron spectroscopy (XPS) experiments were performed on a PHI 5000 Versa Probe high performance electron spectrometer, using monochromatic Al Kα radiation (1486.6 eV) operating at an accelerating power of 15 kW. Before the measurement, the sample was outgassed at room temperature in a UHV chamber ($<5 \times 10^{-7}$ Pa). The sample charging effects were compensated by calibrating all binding energies (BE) with the adventitious C 1s peak at 284.6 eV. This reference gave BE values with an accuracy at ±0.1 eV.

The *in situ* DRIFT experiments were performed on a Nicolet Nexus 5700 FTIR spectrometer by using a diffuse reflectance attachment (HARRICK) equipped with a reaction cell (ZnSe windows). The number of scans was 32 at a resolution of 4 cm^{-1} and the spectra were presented as Kubelka–Munk function referred to background spectra recorded catalyst in N_2. The powder sample was used and pretreated in N_2 at 400 °C for 1 h prior to adsorption experiments. The reaction conditions were as follows: 1000 ppm NH_3, 1000 ppm SO_2, 5 vol.% O_2, N_2 balance. Afterwards, (1) for the co-adsorption of $SO_2 + O_2$, the samples were simultaneously purged by $SO_2 + O_2$ at 300 °C and spectra were collected as a function of time for 1 h, and then collected at 350 and 400 °C after keeping 10 min at every temperature point; (2) for adsorption–desorption of NH_3, NH_3 was adsorbed for 1 h at room temperature, following purged by N_2 for 15 min, then spectra were collected at a desired temperature by the heating rate of 10 °C min^{-1} in flowing N_2; (3) for the adsorption of NH_3 influenced by sulfated at 300 °C, pre-adsorbed $SO_2 + O_2$ for 1 h and collected spectra, following purged by N_2 for 15 min, then purged by NH_3 for 30 min and collected spectra, following purged by N_2 at 400 °C for 10 min, and then decreased to 300 °C and collected spectra.

2.3. Catalytic activity test

Catalytic reaction was performed in a fixed-bed quartz reactor tube. The reaction conditions were: 500 ppm NO, 500 ppm NH_3, 5 vol.% O_2, 200 ppm SO_2 (when used) and 5 vol.% H_2O (when used) with balance N_2, the gas flow rate of 100 ml min^{-1} and 0.1 g sample was used (GHSV of *ca.* 90,000 h^{-1}). Prior to catalytic test, samples were pretreated in N_2 at 200 °C for 1 h. The effluent gases including NO, NH_3, NO_2, and N_2O were continuously analyzed at 150 °C by an online Thermofisher IS10 FTIR spectrometer equipped with a 2 m path-length gas cell (250 ml volume). For catalytic activity as a function of temperature, data was collected at required temperature keeping 15 min when reaction reached a steady state. The NO conversion and N_2 selectivity were calculated by the following equations:

$$\text{NO conversion}\,(\%) = \frac{[NO]_{in} - [NO]_{out}}{[NO]_{in}} \times 100$$

$$N_2\ \text{selectivity}\,(\%) = \frac{[NO]_{in} - [NO]_{out} + [NH_3]_{in} - [NH_3]_{out} - [NO_2]_{out} - 2[N_2O]_{out}}{[NO]_{in} - [NO]_{out} + [NH_3]_{in} - [NH_3]_{out}}$$

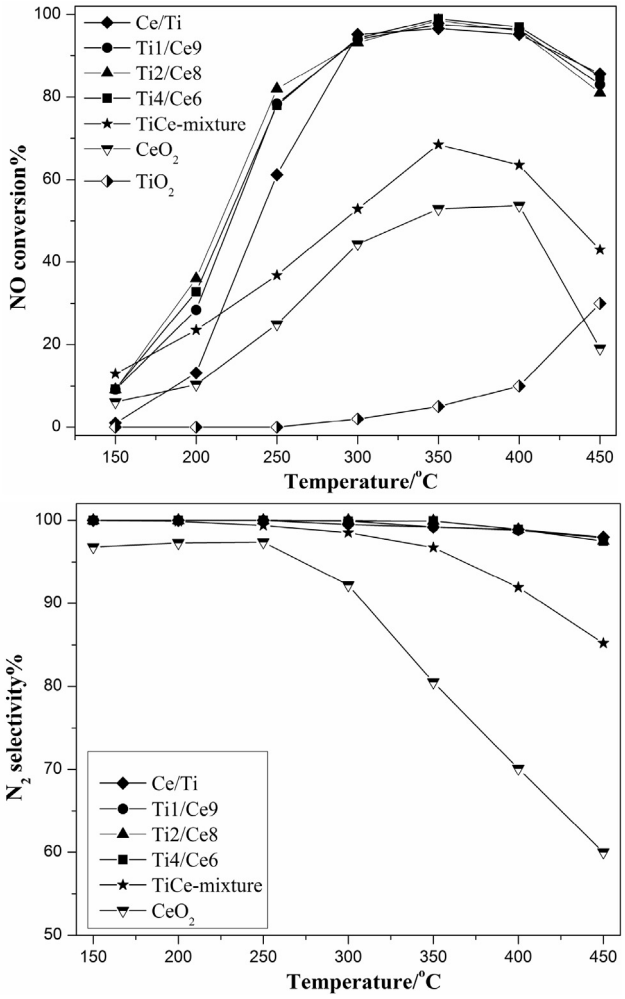

Fig. 1. NO conversion and N_2 selectivity of samples in NH_3-SCR as a function of temperature.

3. Results and discussion

3.1. Catalytic activity results

3.1.1. NH_3-SCR activity results

Fig. 1 shows the results of NO conversion and N_2 selectivity as a function of temperature for NH_3-SCR over the samples. For pure CeO_2 and TiO_2, both of them had bad catalytic activity in NH_3-SCR. When TiO_2 was loaded on CeO_2 or CeO_2 was loaded on TiO_2, except the better catalytic activity of Ti/Ce at 150–250 °C, both Ce/Ti and Ti/Ce samples exhibited similar NH_3-SCR activity with more than 90% NO conversion from 300 to 400 °C and over 97% N_2 selectivity in the entire studied temperatures. It should be noted that the mechanically mixed TiCe sample exhibited much worse NO conversion and N_2 selectivity compared with Ti/Ce and Ce/Ti samples. The catalytic activities of samples followed the order of Ti/Ce ≈ > Ce/Ti > mechanically mixed TiCe > pure CeO_2 > pure TiO_2. As reported elsewhere [24], the Ce–O–Ti short range order species with the interaction between Ce and Ti in atomic scale was the active site for Ce–Ti-based catalysts. In contrast with the mechanically mixed TiCe sample, the supported samples of Ti/Ce and Ce/Ti are more conducive to promote the interaction between CeO_2 and TiO_2 in atomic scale to form the structure of Ce–O–Ti. Since the loading amounts of TiO_2 had no obvious influence on catalytic performances of Ti/Ce samples, Ti1/Ce9 was chosen as a representative in the comparative studies of Ce/Ti and CeO_2.

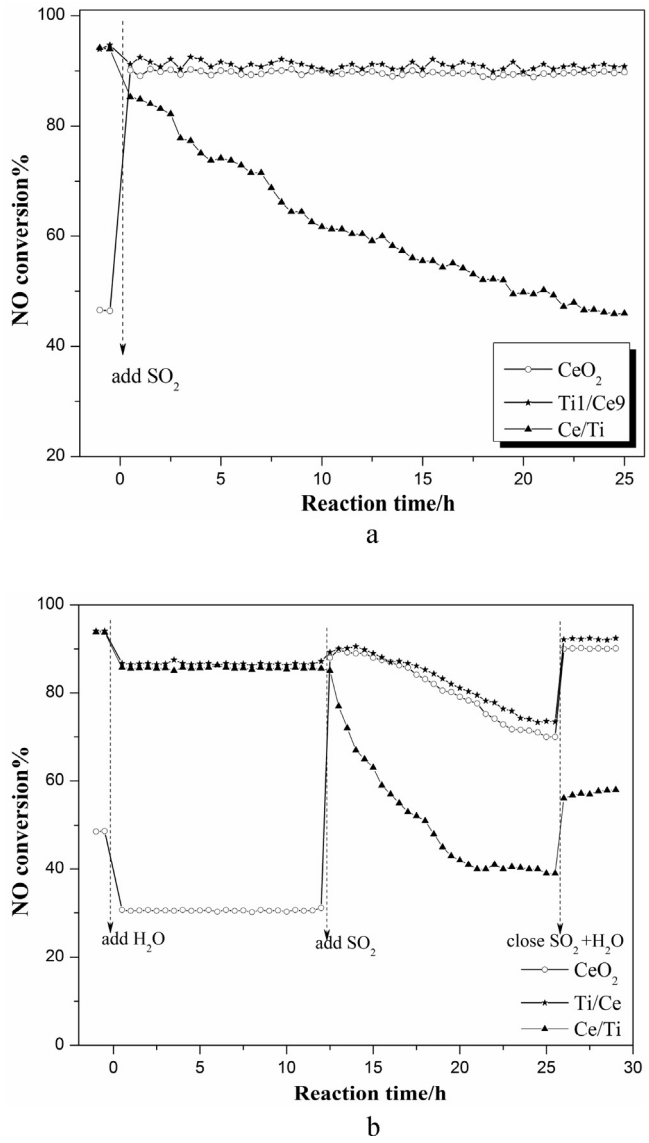

Fig. 2. (a) 200 ppm SO_2 resistance tests and (b) 5 vol.% H_2O or/and 200 ppm SO_2 resistance tests at 300 °C over Ce/Ti, Ti1/Ce9 and CeO_2.

3.1.2. Effect of SO_2 and/or H_2O on NH_3-SCR over CeO_2, Ti1/Ce9 and Ce/Ti

In practical working conditions, especially for coal-fired power plants, the effluent gases always contain a small amount of SO_2 and H_2O [25]. Thus, the influence of SO_2 and H_2O on catalytic performance must be considered for NH_3-SCR catalyst. Fig. 2a shows the results of catalytic activity in the presence of SO_2 over CeO_2, Ti1/Ce9 and Ce/Ti. NO conversion declined continuously from *ca.* 94% to *ca.* 46% during the whole testing for Ce/Ti. While NO conversions of Ti1/Ce9 decreased slightly within 30 min after the injection of SO_2, and NO conversion was maintained at *ca.* 90% in consecutive testing process. Previous research [26] reported that NH_3-SCR activity of CeO_2 could be significantly improved after the sulfation of CeO_2 by SO_2 at 300 °C for 1 h. Thus, we need to further investigate the SO_2 resistance of CeO_2 in order to find out reasons why Ti/Ce has excellent SO_2 resistance. As shown in Fig. 2a, CeO_2 had only about 45% NO removal rate at 300 °C before adding SO_2. With the injection of SO_2 for 30 min, the NO conversion of CeO_2 was over up to *ca.* 90%, which was comparable to the catalytic effect with the pre-sulfation of pure CeO_2 [26]. It is interesting that NO conversion was keeping at *ca.* 90% in the whole testing.

As shown in Fig. 2b, when only 5 vol.% H_2O started to be added, the NO conversions of Ti1/Ce9 and Ce/Ti dropped *ca.* 8% while pure CeO_2 dropped *ca.* 18%, which resulted from the competitive adsorption between H_2O and NH_3 [4]. In the next 12 h, the NO conversions of all samples were almost unchanged. When 200 ppm SO_2 was added after passing into H_2O 12 h, for pure CeO_2 and Ti1/Ce9, the NO conversion firstly increased to *ca.* 90% and then gradually declined *ca.* 74% for Ti1/Ce9 and *ca.* 70% for pure CeO_2 at 25 h. While for Ce/Ti, the NO conversion continued to decline to 39%. In addition, once SO_2 and H_2O were closed, NO conversion of pure CeO_2 and Ti1/Ce9 could quickly recover to *ca.* 90% while just recovered to *ca.* 57% for Ce/Ti.

From the results of SO_2 and H_2O resistance tests, it can be summed up that: (1) Ti1/Ce9 exhibits much better SO_2 resistance than Ce/Ti; (2) CeO_2 shows the poor NH_3-SCR activity without SO_2, but once SO_2 is introduced, the catalytic activity is extremely improved, and SO_2 resistance of CeO_2 is nearly as good as that of Ti1/Ce9; (3) the catalytic activities of Ti1/Ce9 and Ce/Ti are slightly influenced when only H_2O is introduced; (4) although the deactivation of Ce/Ti is irreversible in the co-presences of SO_2 and H_2O, the deactivation of CeO_2 and Ti1/Ce9 is reversible. Meanwhile, it can be seen that SO_2 has more significant inhibitory effect on NH_3-SCR catalytic activity than H_2O based on the configuration differences of Ce–Ti-based catalysts. Combined with the NH_3-SCR promotional effect of sulfation over pure CeO_2, we focus on the differences of SO_2 resistance between Ti/Ce and Ce/Ti, and try to understand the interaction mechanism between SO_2 and Ce–Ti-based catalysts.

3.2. Characterization

3.2.1. TG-DTA results

The used samples were measured by TG-DTA to analyze surface species formed in the tests with SO_2. As shown in Fig. 3, the weight losses of all the used samples could be divided into three steps. Step I (25–200 °C) could be mainly assigned to the desorption of adsorbed water on the samples. Previous studies demonstrated that pure NH_4HSO_4 started to decompose at about 390 °C while pure $(NH_4)_2SO_4$ decomposed at 280 °C [27]. Since the used samples were reacted at 300 °C, Step II (200–550 °C) mainly contained the decomposition of NH_4HSO_4 formed by the reaction among NH_3, SO_2 and H_2O. The fresh pure CeO_2 and Ce/TiO_2 samples did not have obvious decomposition or desorption behavior above 550 °C [19,28], but the weight losses of Step III (550–800 °C) for the used samples were still observed. It is reported that the decomposition temperature of $Ce(SO_4)_2$ and $Ce_2(SO_4)_3$ over Ce/TiO_2 was higher than 700 °C by SO_2-TPD [19]. Therefore, Step III of used samples could be assigned to the decomposition of $Ce(SO_4)_2$ and/or $Ce_2(SO_4)_3$ formed by chemisorption between SO_2 and CeO_2.

3.2.2. XRD and BET results

Fig. 4a shows XRD results of the fresh samples. For Ce/Ti, all peaks were assigned to anatase-type phase TiO_2 (PDF-ICDD 84-1286) except the peak at 28.6° which was cubic fluorite-type phase CeO_2 (PDF-ICDD 34-0394). Ti1/Ce9 only had peaks of CeO_2, indicating that TiO_2 highly dispersed on the surface of CeO_2. When the molar ratio of Ti/Ce was over 2:8, peak at 25.3° appeared indicating the formation of crystalline anatase TiO_2. For the used samples, as shown in Fig. 4b, the diffraction patterns of all samples had no obvious change compared with the fresh samples.

The surface area data of fresh and used samples are listed in Table 1. For the fresh samples, both Ce/Ti and Ti1/Ce9 had similar surface area. While the surface area of used samples decreased, which was possibly correlated with sulfate species covered on the surface of used samples. It should be noted that the descent rate of surface area (ΔS) of CeO_2-U (47.5%) was greater than that of Ti1/Ce9-U (23.0%), which indicates that TiO_2 loaded on CeO_2 is

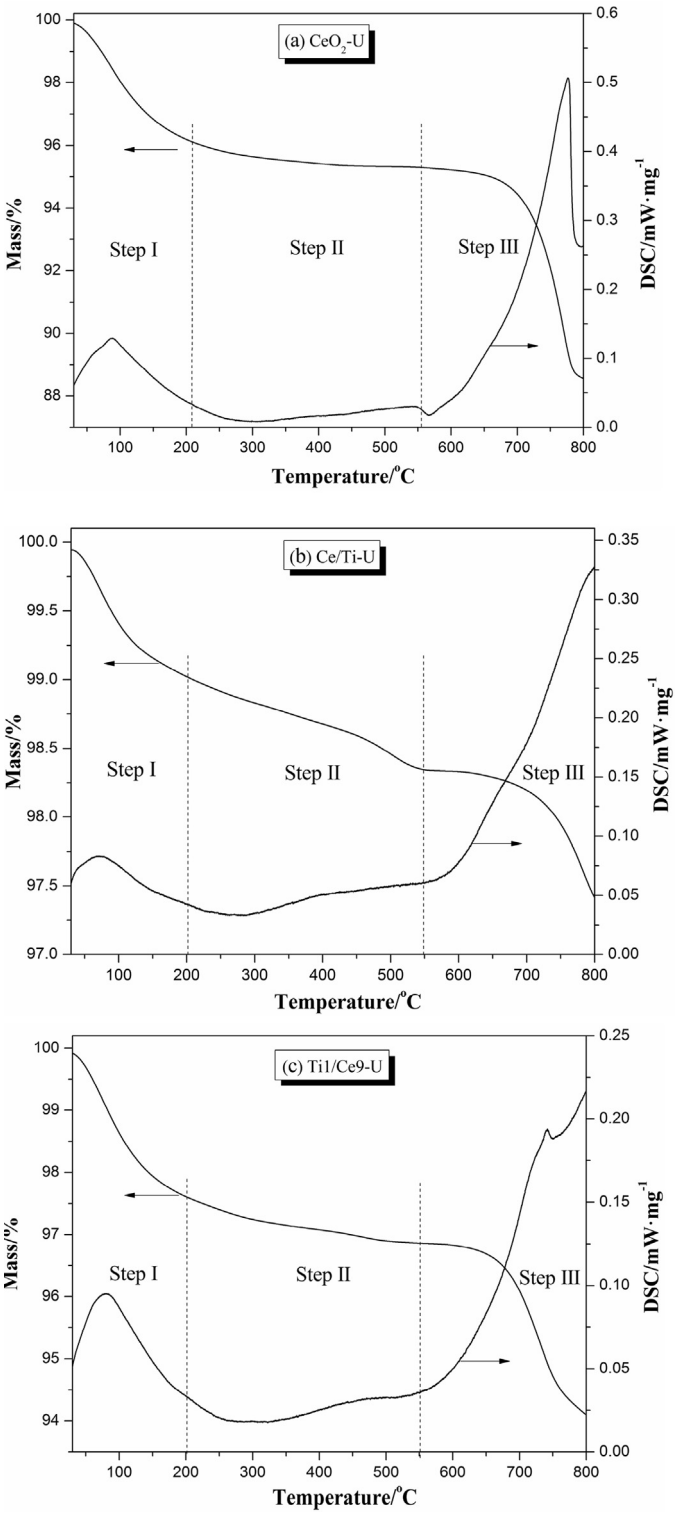

Fig. 3. TG-DTA curves of used catalysts: (a) CeO_2-U; (b) Ce/Ti-U; (c) Ti1/Ce9-U.

Table 1
The surface area of fresh and used samples.

Samples	Fresh S_1 ($m^2\ g^{-1}$)	Used S_2 ($m^2\ g^{-1}$)	$\Delta S = \frac{S_1 - S_2}{S_1}$ (%)
CeO_2	69.5	36.5	47.5
Ce/Ti	47.3	38.6	18.4
Ti1/Ce9	49.1	37.8	23.0

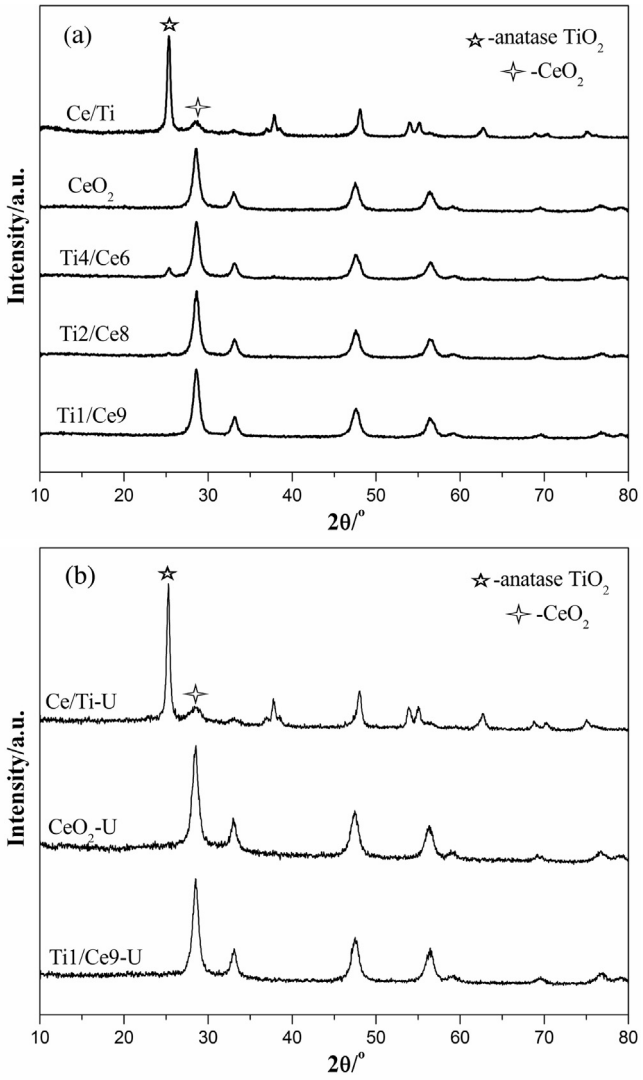

Fig. 4. XRD results of fresh samples (a) and used samples (b).

beneficial to restrain the influence of sulfates on the surface area of CeO_2.

3.2.3. *In situ* DRIFT results

The co-adsorption DRIFT of $SO_2 + O_2$ at 300 °C was conducted to investigate the existence states of sulfates for understanding the interaction between sulfates and samples. In the region of 900–1400 cm^{-1} as shown in Fig. 5, these bands could be mainly related to the vibrations of chelating bidentate sulfates (SO_4^{2-}). According to previous studies [29–31], bands at 997–1003 and 1102–1105 cm^{-1} could be assigned to the symmetric stretching frequencies of O–S–O species, while bands at 1310–1314 and 1354–1363 cm^{-1} could be attributed to the asymmetric stretching frequencies of O=S=O species for surface sulfates adsorbed on metal oxide. A broad band at 1180 cm^{-1} over pure CeO_2 and Ce/Ti appeared and enhanced with the increase of adsorption time. Bands at 1160–1200 cm^{-1} were found on CeO_2 and CeZrO solid solution [30,32,33], which were ascribed to sulfates located in bulk or subsurface of CeO_2 and CeZrO solid solution (bulk-like sulfates). Therefore, the band at 1180 cm^{-1} observed in our experiment could be assigned to bulk-like sulfates in CeO_2. It is worth noting that the band at 1180 cm^{-1} in pure CeO_2 enhanced with the increase of temperature from 300 to 400 °C, indicating that more bulk-like sulfates were formed at high temperature. It is also reported [30]

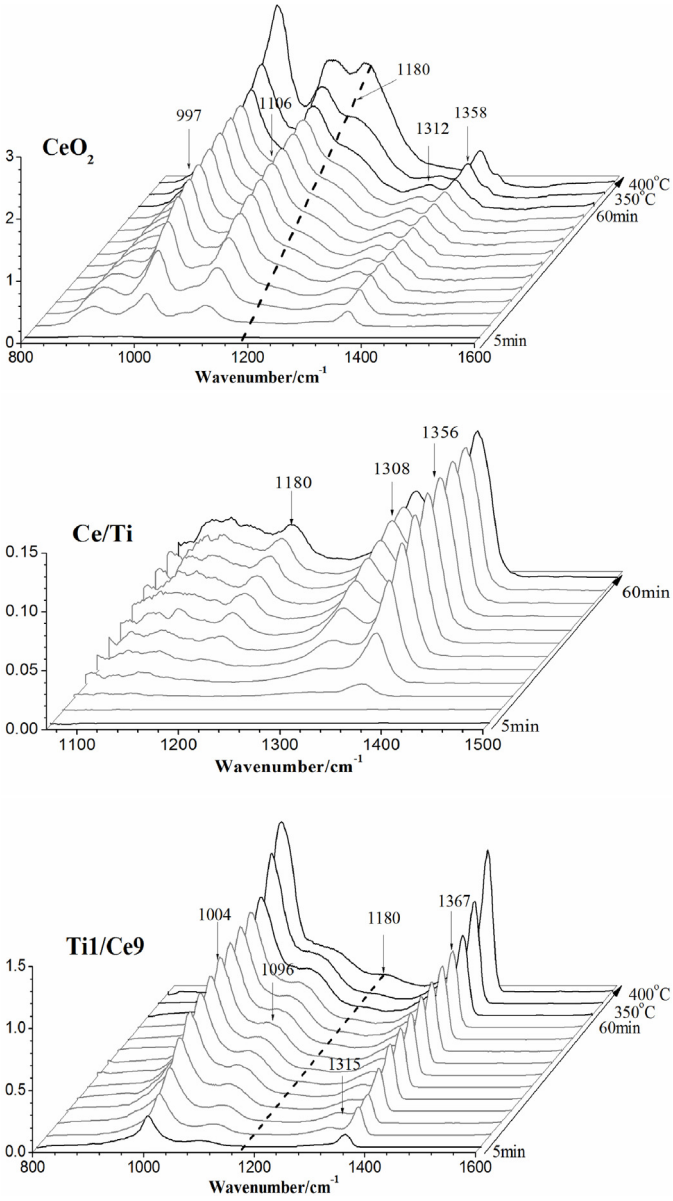

Fig. 5. *In situ* DRIFT $SO_2 + O_2$ co-adsorption spectra over CeO_2, Ce/Ti and Ti1/Ce9 at 300 °C as a function of time for 60 min, 350 and 450 °C for 10 min.

that the formation of more bulk-like sulfates was favored at higher temperature. Since bulk CeO_2 appeared over Ce/Ti as proved by XRD, the band at 1180 cm^{-1} due to bulk-like sulfates could be also detected over Ce/Ti. Interestingly, bands of surface adsorbed sulfates obviously exhibited over Ti1/Ce9, but no band of bulk-like sulfates could be observed at 300 °C and just a weak band at 1180 cm^{-1} due to bulk-like sulfates appeared at 400 °C. This indicates that the reaction between SO_2 and CeO_2 in the presence of O_2 was inhibited probably by the dispersed TiO_2 species, and the formation of bulk-like sulfates in Ti1/Ce9 was more difficult than that in pure CeO_2. Thus, it can be concluded that the sulfation at 300 °C results in the formation of two different kinds of sulfate species, including surface sulfates for all samples and bulk-like sulfates for CeO_2 and Ce/Ti.

Fig. 6 shows the results of NH_3 adsorption–desorption DRIFT over the fresh samples as a function of temperature. For pure CeO_2, the bands at 1565, 1296, 1138, 1118 and 1057 cm^{-1} could be ascribed to NH_3 coordinated to Lewis acid sites (denoted as L acids) [31,34]. L acids over CeO_2 were weak adsorption as the

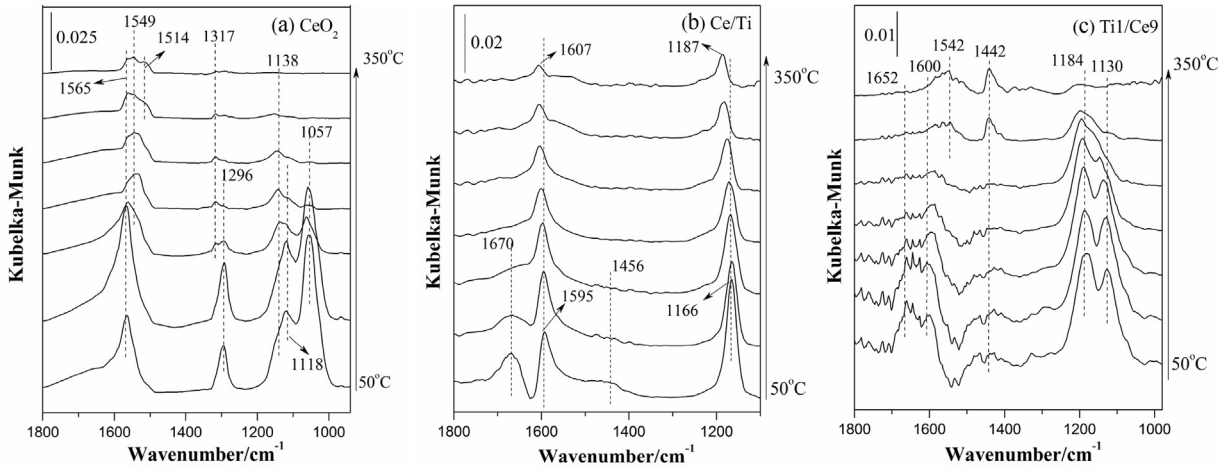

Fig. 6. *In situ* DRIFT NH_3 adsorption–desorption spectra of CeO_2, Ce/Ti and Ti1/Ce9 as a function of temperature.

bands of L acids suddenly dropped at 200 °C and completely vanished at 350 °C. Meanwhile, the bands at 1549 and 1317 cm^{-1} due to the NH_2 species were formed after the temperature increased to 150 °C [35,36]. With regard to Ce/Ti, L acids at 1595 and 1166 cm^{-1} gradually desorbed and still existed at 350 °C while bands at 1670 and 1456 cm^{-1} assigned to Brønsted acids (denoted as B acids) eliminated at 200 °C [20,37]. Nevertheless, for Ti1/Ce9, the bands at 1652 and 1442 cm^{-1} due to B acids existed for the whole experimental procedure. Interestingly, Ti1/Ce9 emerged two bands corresponding to L acids at 1184 and 1130 cm^{-1}. Considering the NH_3 adsorption on pure TiO_2 formed a band of L acid at about 1180 cm^{-1} (not shown), it can be deduced that two kinds of L acid sites exist over Ti1/Ce9: one is from the dispersed Ti^{4+} for 1184 cm^{-1} and the other one is from bulk CeO_2 for 1130 cm^{-1}. Nevertheless, L acid sites were mainly provided by TiO_2 for Ce/Ti.

In order to further investigate the influence of sulfation on NH_3 adsorption, NH_3 adsorption–desorption DRIFT of sulfated samples were conducted. As shown in Fig. 7, curve A was collected by the sulfation of samples for 1 h. After injecting NH_3 for 30 min for all samples (Fig. 7 curves B), a new band at 1420–1440 cm^{-1} appeared, which could be assigned to the asymmetric bending vibrations of ionic NH_4^+ bounded to Brønsted acid sites provided by surface sulfates [37–39]. At the same time, accompanied by the appearance of new band at 1241–1275 cm^{-1}, the intensity of bands at 1310–1314 and 1354–1363 cm^{-1} due to O=S=O groups obviously decreased. Results of the regular DRIFT of NH_4HSO_4 deposited on CeO_2, Ce/Ti and Ti1/Ce9 (Fig. S1) show that band at *ca.* 1255 cm^{-1} was the characteristic vibration peak of HSO_4^- species, which also could be observed on CeO_2 at 1275 cm^{-1}, on Ce/TiO_2 at 1257 cm^{-1} and on Ti1/Ce9 at 1241 cm^{-1}. Thus, it indicates that NH_4HSO_4 was formed on the three sulfated samples by the introduction of NH_3. When samples were purged by N_2 for 10 min at 400 °C (Fig. 7 curves C), the bands of HSO_4^- at 1241–1275 cm^{-1} and NH_4^+ at 1420–1440 cm^{-1} obviously decreased with the reappearance of surface sulfates at about 1360 cm^{-1}. These results indicate that NH_4HSO_4 deposited on samples has decomposed by thermal treatment at 400 °C and converted to surface adsorbed sulfates accompanying with the desorption of NH_3. Therefore, based on the results of TG-DTA and *in situ* DRIFT, it is reasonable to deduce that in the presence of SO_2 at 300 °C for NH_3-SCR, NH_4HSO_4, metal sulfates (surface and/or bulk-like sulfates) are formed over the studied samples.

3.2.4. XPS results

XPS experiments were carried out to investigate the surface component and chemical state change of elements over the fresh and used samples. The corresponding results were displayed in Fig. 8, and the peaks were fitted by Gaussian–Lorentz curves. The surface atomic concentrations, atomic ratios of $Ce^{3+}/(Ce^{3+}+Ce^{4+})$ and different oxygen species obtained by Gaussian–Lorentz fitting were listed in Table 2. For the bands of Ti 2p over either the fresh or used samples, no obvious change happened (Fig. 8a). It is worth noting that the photoemission of S 2p could be detected over the used samples (Fig. 8b), and the binding energy of S 2p, 168.8 eV, was corresponding to the S(VI) oxidation state [19,40], which indicates that sulfate species were formed in the NH_3-SCR tests with SO_2. Combined with DRIFT results, it is reasonable to believe that the sulfur measured by XPS derived from NH_4HSO_4 and metal sulfates on the surface of samples. It can be seen from Table 2, the surface sulfur concentration of Ti1/Ce9 was lower than that of pure CeO_2, which indicates that the reactions between SO_2 and CeO_2 or NH_3 to generate sulfate species were inhibited by the dispersed TiO_2 species.

The complex spectra of Ce 3d were decomposed into eight components by Gaussian–Lorentz fitting procedure (Fig. 8c). The bands labeled *u* were due to $3d_{3/2}$ spin-orbit states and those labeled *v* represented $3d_{5/2}$ states. The bands labeled as *u′* and *v′* were ascribed to the primary photoemission of Ce^{3+} and the other six bands labeled as *u‴* and *v‴*, *u″* and *v″*, and *u* and *v* were assigned to Ce^{4+} [41,42]. The fitting results reveal that both Ce^{3+} and Ce^{4+} existed in all samples. Combined with the results of SO_2+O_2 DRIFT, it indicates that the chemisorption between sulfates and CeO_2 mainly formed $Ce(SO_4)_2$ and $Ce_2(SO_4)_3$. Moreover, the ratios of $Ce^{3+}/(Ce^{3+}+Ce^{4+})$ over the used samples were greater than that of the corresponding fresh samples as listed in Table 2. This is because SO_2 reacted with CeO_2 in the presence of O_2 as following reaction [40,43]:

$$2CeO_2+3SO_2+O_2= Ce_2(SO_4)_3$$

For oxygen species (Fig. 8d), O′ was ascribed to surface oxygen species and O″ was attributed to the lattice oxygen of metal oxides [31]. Compared with Ce/Ti, either the fresh or used samples, the band of lattice oxygen O″ for Ti1/Ce9 moved toward lower binding

Table 2
The surface components of fresh and used samples obtained by XPS analysis.

Samples	Atomic concentration (mol.%)				Atomic ratio (%)	
	Ce	Ti	O	S	$Ce^{3+}/(Ce^{3+}+Ce^{4+})$	O′/(O′ +O″)
Ce/Ti	1.8	24.5	73.7	–	19.4	18.6
Ti1/Ce9	19.1	7.2	73.7	–	15.8	26.6
Ce/Ti-U	1.7	23.5	72.7	2.1	36.7	25.6
Ti1/Ce9-U	17.4	6.1	72.9	3.6	23.0	36.9
CeO_2-U	22.6	–	73.1	4.3	24.2	42.9

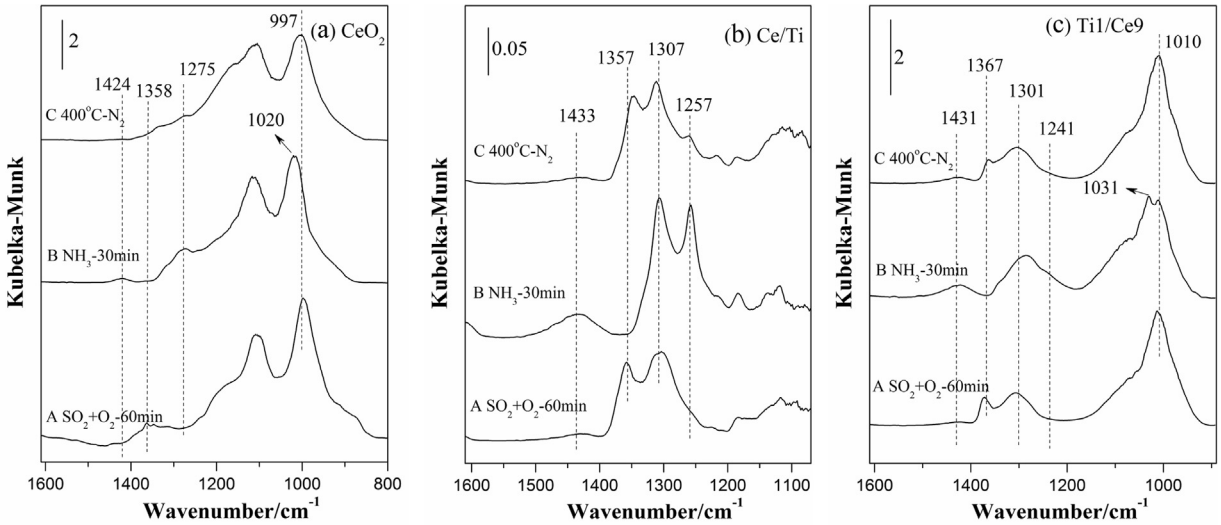

Fig. 7. *In situ* DRIFT spectra of reaction between NH_3 and the adsorbed sulfates over CeO_2, Ce/Ti and Ti1/Ce9. (A) $SO_2 + O_2$ co-adsorption for 60 min at 300 °C; (B) NH_3 adsorption for 30 min after (A) at 300 °C; (C) purging N_2 at 400 °C for 10 min after (B).

energy, as the binding energy of lattice oxygen of CeO_2 was lower than that of TiO_2 [42]. In addition, comparing to the fresh samples, the corresponding used samples contained more surface oxygen species, which was related to sulfates formed over the used samples. While the amount of surface oxygen species over Ti1/Ce9 was smaller than that of pure CeO_2, which suggests that the formation of sulfate species over CeO_2 could be inhibited by the dispersed TiO_2 species.

3.2.5. H_2-TPR results

Fig. 9a shows H_2-TPR results of fresh samples. Ce/Ti had a broad peak at *ca.* 650 °C mainly including the reduction of dispersed CeO_2, bulk CeO_2 and TiO_2. The reduction behaviors of Ti/Ce samples were similar to that of CeO_2. Peaks α, β and γ could be respectively assigned to the reduction of surface active oxygen species, subsurface layers or deeper interior of CeO_2 and bulk CeO_2 (for Ti/Ce samples, peaks β and γ also contained the reduction of TiO_2) [44,45]. For peak α, the loading amount of TiO_2 to CeO_2 had no influence on the peak temperature. However, compared with pure CeO_2, the peaks β of Ti/Ce samples moved backward to about 60 °C and peaks γ moved forward to about 20 °C. It can be considered that the interaction between TiO_2 and CeO_2 by Ti–O–Ce over Ti/Ce samples could impact on the reduction behavior of CeO_2 [24,42].

In order to investigate the effect of SO_2 on the redox performance of samples, the used samples were characterized by H_2-TPR. As shown in Fig. 9b, compared with the fresh samples, the used samples had a strong peak at range from 550 to 625 °C, which mainly contained the reduction of sulfate species [30,37]. Therefore, the peaks from 300 to 650 °C for the used samples contained the reduction of both sulfate species and subsurface layers or deeper interior of CeO_2. Since TG-DTA results indicate that NH_4HSO_4 has decomposed over samples before 550 °C, and DRIFT results confirm that sulfates formed by the decomposition of NH_4HSO_4 could be adsorbed on samples to form metal sulfates again. Thus, the strong peaks measured by TPR primarily contained sulfate species from metal sulfates and NH_4HSO_4. Since it is difficult to distinguish the reduction amount of sulfate species from that of subsurface layers or deeper interior of CeO_2, the peak areas from 300 to 650 °C were fitted to estimate the relative amounts of sulfate species over the used samples (Table 3). Meanwhile, the relative amounts of sulfate species were calculated by weight loss ratios (Step III) of TG-DTA for the used samples (Table 3). Both TPR and TG-DTA results indicate that the amounts of sulfate species followed the order of CeO_2 > Ti1/Ce9 > Ce/Ti. Previous studies reported that sulfates weakly adsorbed on TiO_2 [46] and could completely desorb before 300 °C [47]. Hence, it can be seen that metal sulfates in all samples consisted of $Ce(SO_4)_2$ and $Ce_2(SO_4)_3$. Furthermore, the reduction peak temperature of sulfate species increased following the order of CeO_2 > Ti1/Ce9 > Ce/Ti, which could be explained by the different existence states of sulfate species in samples. On one hand, bulk-like sulfates in pure CeO_2 are more difficult to be reduced than surface sulfates; on the other hand, the interactions between surface sulfates and CeO_2 can be weakened by Ce–O–Ti in Ce/Ti and Ti/Ce.

3.3. Proposed adsorption model of SO_2 over Ce–Ti-based catalysts

Generally speaking, good NH_3-SCR catalytic performances of catalysts derive from synergistic catalysis between acid sites and redox sites. For the studied samples, there are mainly two reaction routes over the sulfated samples (Fig. 10). Route I proceeds via the active sites of surface sulfates and bulk CeO_2 over sulfated CeO_2, in which surface sulfates work as acid sites and bulk CeO_2 provides redox sites [37]. Route II proceeds via the active sites of Ce–O–Ti over Ce/Ti and Ti/Ce samples as discussed in Subsection 3.1.1. Generally, SO_2 poisoning of catalysts happens mainly in two different ways. In NH_3-SCR process with the existence of SO_2, SO_2 can be catalytically oxidized to SO_3 by NH_3-SCR catalysts, and then SO_3 can react with catalyst to form stable metal sulfates or react with gas species (mainly NH_3 and H_2O) to form stable NH_4HSO_4. While, both metal sulfates and NH_4HSO_4 might block active sites and result in the decline of catalytic performance [48,49]. Herein, 5 wt.% NH_4HSO_4 was deposited on CeO_2, Ce/Ti and Ti1/Ce9 and NH_3-SCR performance tests were conducted (Fig. S2). The catalytic activity of CeO_2 deposited NH_4HSO_4 (CeO_2-N) notably enhanced comparing to pure CeO_2. This is because B acids can be formed by the adsorption of HSO_4^-, which exhibits the same catalytic

Table 3
The relative amounts of sulfate species for the used samples obtained by TG-DTA and TPR.

Samples	Ce/Ti-U	Ti1/Ce9-U	CeO_2-U
Sulfates by TG-DTA[a]	1.0	3.7	7.9
Sulfates by TPR[a]	1.0	5.9	8.4

[a] The ratio was normalized by Ce/Ti-U.

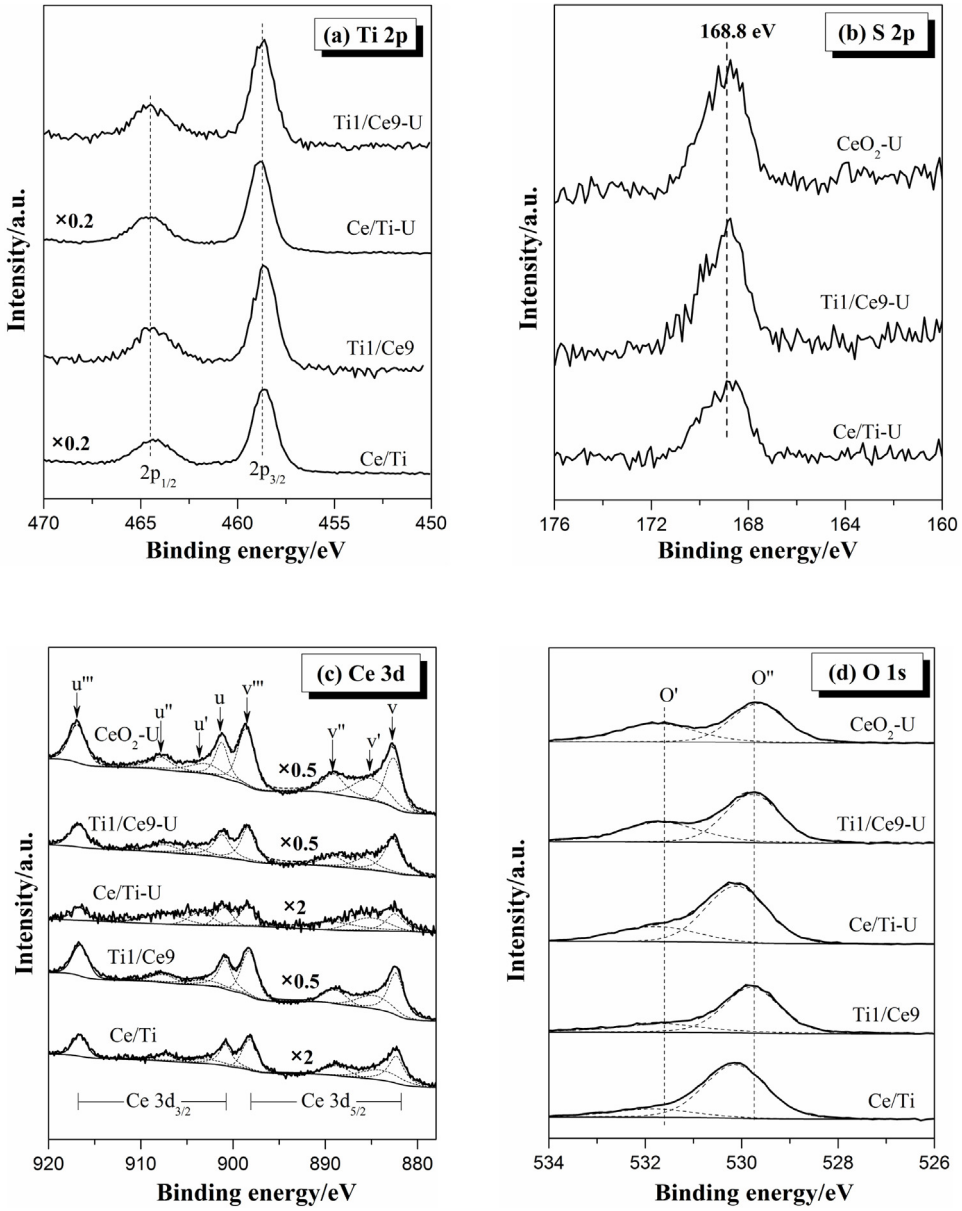

Fig. 8. XPS results of Ti 2p (a), S 2p (b), Ce 3d (c) and O 1s (d) over the fresh and used samples.

effect with the sulfation of pure CeO_2 mentioned in Subsection 3.1.2. NH_4HSO_4 had no obvious influence on catalytic activity for Ti1/Ce9. However, the catalytic activity at 300 °C decreased *ca.* 20% after depositing NH_4HSO_4 on Ce/Ti. When reaction temperature exceeded 350 °C, the activity of Ce/Ti–N was the same as the fresh Ce/Ti sample. Based on results of NH_3-SCR performance showed in Fig. S2, NH_4HSO_4 only inhibited the catalytic activity of Ce/Ti at low temperature, but had no negative effect on the catalytic activity of Ti1/Ce9. Moreover, the presence of NH_4HSO_4 even improved the catalytic activity of pure CeO_2 sample. Thus, the possibility that the deposition of NH_4HSO_4 on the studied samples is main reason for deactivation at 300 °C can be ruled out. For Ce–Ti-based catalysts, the deactivation is mainly caused by the formation of metal sulfates mainly including $Ce(SO_4)_2$ and $Ce_2(SO_4)_3$ species.

Combined with the results of catalytic activity and *in situ* DRIFT, we propose the adsorption model of SO_2 to explain the differences of SO_2 resistance over CeO_2, Ce/Ti and Ti/Ce. As shown in Fig. 10a, in the presence of SO_2 and O_2 at 300 °C, pure CeO_2 can be sulfated to form surface sulfates and some bulk-like sulfates. NH_3-SCR can proceed via the synergistic catalysis between surface sulfates and bulk CeO_2 (by route I). However, for Ce/Ti (Fig. 10b), as sulfates adsorb on the loaded CeO_2 to form metal sulfates and block the active site of Ce–O–Ti, so route II can be inhibited to result in the irreversible deactivation. With regard to Ti/Ce (Fig. 10c), sulfation only takes place on the surface, although the active sites of Ce–O–Ti are blocked by surface sulfates (null by route II), NH_3-SCR reaction can proceed via synergistic catalysis between surface sulfates and bulk CeO_2 (by route I).

In order to validate the proposed models, samples were sulfated by the pretreatment of $SO_2 + O_2$. As shown in Fig. 11, the catalytic activity of sulfated Ce/Ti significantly declined comparing to the fresh Ce/Ti, and sulfated temperatures had minor influence on catalytic activity. This is because $Ce(SO_4)_2$ and $Ce_2(SO_4)_3$ species on the surface of Ce/Ti were formed at both sulfated temperatures, and blocked the active sites of Ce–O–Ti. When Ti/Ce and pure CeO_2 were sulfated at 250 °C, both of them exhibited good catalytic activity as reaction could proceed by route I. Interestingly, the activity of Ti/Ce and CeO_2 declined when sulfated at 450 °C, while the activity

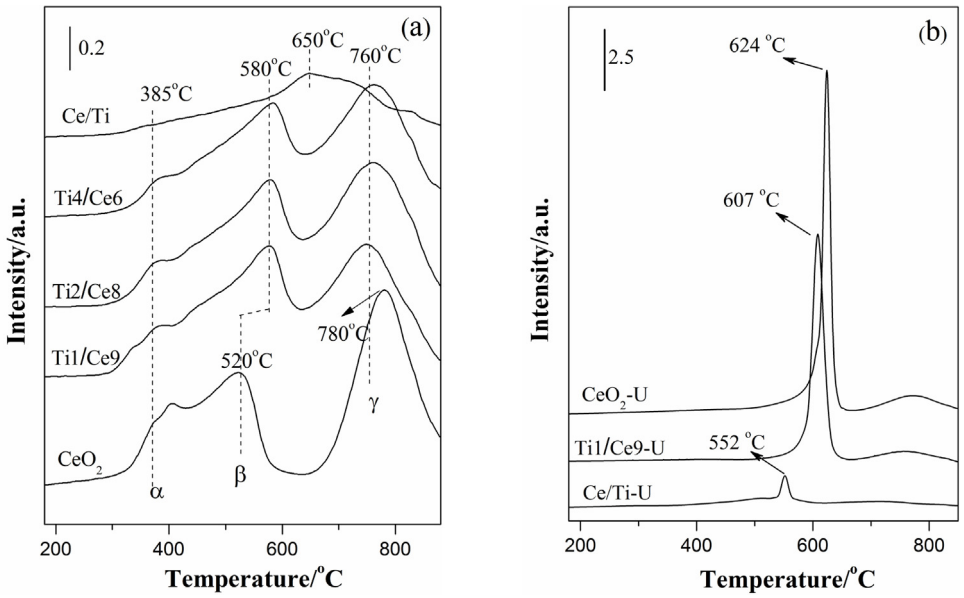

Fig. 9. H_2-TPR results of fresh samples (a) and used samples (b).

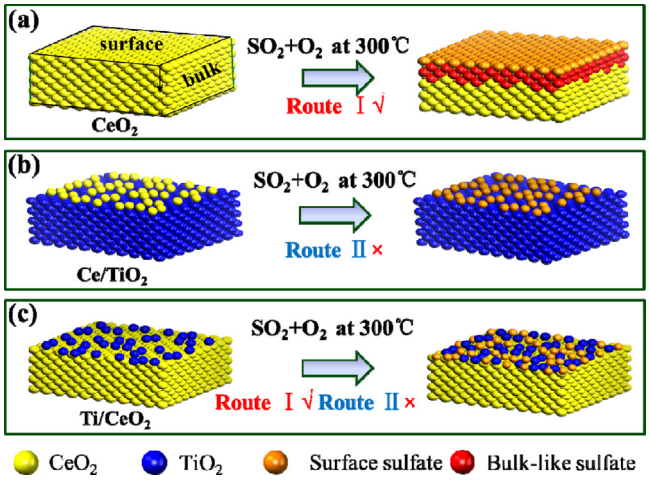

Fig. 10. Proposed adsorption model of SO_2 over CeO_2, Ce/Ti and Ti/Ce.

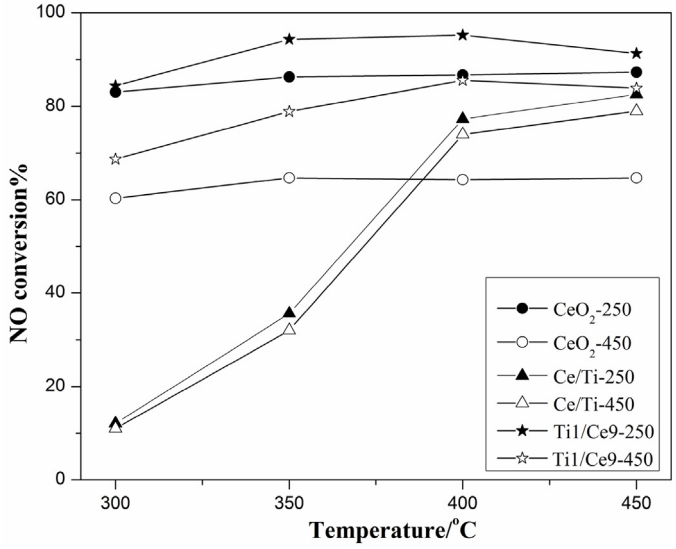

Fig. 11. NH_3-SCR activities of CeO_2, Ce/Ti and Ti1/Ce9 pretreated by 1000 ppm SO_2 with 5 vol.% O_2 at 250 or 450 °C for 1 h.

of Ti/Ce was still better than that of Ce/Ti. Based on *in situ* DRIFT results of $SO_2 + O_2$, one possible reason for the influence of sulfated temperature on the activity of CeO_2 and Ti/Ce is that bulk CeO_2 was sulfated in depth at higher temperature. However, pure CeO_2 is prone to form more bulk-like sulfates than Ti/Ce, which can inhibit the synergistic catalysis between surface sulfates and bulk CeO_2. Thus, the results of sulfated experiments also supported the SO_2 resistance model of catalysts proposed above.

4. Conclusions

Based on comprehensive characterizations, the influence of configurations of Ce–Ti-based catalysts on SO_2 resistance was studied. Several major conclusions can be obtained as follows:

(1) Both Ce/Ti and Ti/Ce show satisfactory catalytic activity at 300–400 °C in the absence of SO_2, while in the presence of SO_2 and/or H_2O, the activity of Ti/Ce is much better than that of Ce/Ti, and SO_2 has more significant inhibitory effect on $deNO_x$ activity than H_2O based on the configuration differences of Ce–Ti-based catalysts.
(2) TG-DTA and *in situ* DRIFT results indicate that the sulfation of samples under reactive conditions generates three different kinds of sulfate species including NH_4HSO_4, surface and bulk-like metal sulfates. Meanwhile, XPS and H_2-TPR results corroborate that metal sulfates mainly consist of $Ce(SO_4)_2$ and $Ce_2(SO_4)_3$.
(3) The performance of SO_2 resistance can be significantly influenced by the configurations of Ce–Ti-based catalysts. In the presence of SO_2, the formed metal sulfates block the active sites of Ce–O–Ti, which is mainly responsible for the irreversible deactivation of Ce/Ti. While for Ti/Ce, although the active sites of Ce–O–Ti are blocked by metal sulfates, NH_3-SCR can still take place via the synergistic catalysis between surface sulfates and bulk CeO_2.

Acknowledgments

The financial supports of the National Natural Science Foundation of China (Nos. 21273110, 21203091), Doctoral Fund of Ministry of Education of China (No. 2013009111005), the National Basic

Research Program of China (973 program, No. 2010CB732300) and the valuable technique help of Dr. Xi Hong are gratefully acknowledged.

Appendix A. Supplementary data

Supplementary data associated with this article can be found, in the online version, at http://dx.doi.org/10.1016/j.apcatb.2014.10.029.

References

[1] G. Buscaa, L. Liettib, G. Ramisa, F. Berti, Appl. Catal. B: Environ. 18 (1998) 1–36.
[2] P.G. Smirniotis, D.A. PenÄ., B.S. Uphade, Angew. Chem. Int. Edit. 40 (2001) 2479–2481.
[3] P. Forzatti, Appl. Catal. A: Gen. 222 (2001) 221–236.
[4] J.H. Li, H.Z. Chang, L. Ma, J.M. Hao, R.T. Yang, Catal. Today 175 (2011) 147–156.
[5] M.F. Fu, C. Li, P. Lu, L. Qu, M.Y. Zhang, Y. Zhou, M.G. Yu, Y. Fang, Catal. Sci. Technol. 4 (2014) 14–25.
[6] R.Q. Long, R.T. Yang, J. Am. Chem. Soc. 121 (1999) 5595–5596.
[7] M. Colombo, I. Nova, E. Tronconi, Catal. Today 151 (2010) 223–230.
[8] P.S. Metkar, M.P. Harold, V. Balakotaiah, Appl. Catal. B: Environ. 111–112 (2012) 67–80.
[9] W.Q. Xu, Y.B. Yu, C.B. Zhang, H. He, Catal. Commun. 9 (2008) 1453–1457.
[10] X. Gao, Y. Jiang, Y. Zhong, Z.Y. Luo, K.F. Cen, J. Hazard. Mater. 174 (2010) 734–739.
[11] F.D. Liu, H. He, C.B. Zhang, Chem. Commun. (2008) 2043–2045.
[12] F.D. Liu, H. He, Y. Ding, C.B. Zhang, Appl. Catal. B: Environ. 93 (2009) 194–204.
[13] A. Karami, V. Salehi, J. Catal. 292 (2012) 32–43.
[14] X.L. Mou, B.S. Zhang, Y. Li, L. Yao, X.J. Wei, D.S. Su, W.J. Shen, Angew. Chem. Int. Edit. 51 (2012) 2989–2993.
[15] Y. Li, H. Cheng, D. Li, Y. Qin, Y. Xie, S. Wang, Chem. Commun. (2008) 1470–1472.
[16] L. Chen, J. Li, W. Ablikim, J. Wang, H.Z. Chang, L. Ma, J.Y. Xu, M.F. Ge, H. Arandiyan, Catal. Lett. 141 (2011) 1859–1864.
[17] H.Q. Wang, X.B. Chen, X.L. Weng, Y. Liu, S. Gao, Z.B. Wu, Catal. Commun. 12 (2011) 1042–1045.
[18] W.P. Shan, F.D. Liu, H. He, X.Y. Shi, C.B. Zhang, ChemCatChem 3 (2011) 1286–1289.
[19] W.Q. Xu, H. He, Y.B. Yu, J. Phys. Chem. C 113 (2009) 4426–4432.
[20] W.P. Shan, F.D. Liu, H. He, X.Y. Shi, C.B. Zhang, Appl. Catal. B: Environ. 115–116 (2012) 100–106.
[21] Y. Shen, Y. Ma, S. Zhu, Catal. Sci. Technol. 2 (2012) 589–599.
[22] C. Liu, L. Chen, J.H. Li, L. Ma, H. Arandiyan, Y. Du, J.Y. Xu, J.M. Hao, Environ. Sci. Technol. 46 (2012) 6182–6189.
[23] X. Gao, Y. Jiang, Y.C. Fu, Y. Zhong, Z.Y. Luo, K.F. Cen, Catal. Commun. 11 (2010) 465–469.
[24] P. Li, Y. Xin, Q. Li, Z.P. Wang, Z.L. Zhang, L.R. Zheng, Environ. Sci. Technol. 46 (2012) 9600–9605.
[25] R.K. Srivastava, C.A. Miller, C. Erickson, R.J. Jambhekar, Air Waste Manage. 54 (2004) 750–762.
[26] T.T. Gu, Y. Liu, X.L. Weng, H.Q. Wang, Z.B. Wu, Catal. Commun. 12 (2010) 310–313.
[27] Z.P. Zhu, H.X. Niu, Z.Y. Liu, S.J. Liu, J. Catal. 195 (2000) 268–278.
[28] L. Qi, Q. Yu, Y. Dai, C.J. Tang, L.J. Liu, H.L. Zhang, F. Gao, L. Dong, Y. Chen, Appl. Catal. B: Environ. 119–120 (2012) 308–320.
[29] T. Yamaguchi, T. Jin, K. Tanabe, J. Phys. Chem. 90 (1986) 3148–4152.
[30] M. Waqif, P. Bazin, O. Saur, J.C. Lavalley, G. Blanchard, O. Touret, Appl. Catal. B: Environ. 11 (1997) 193–205.
[31] T. Jin, T. Yamaguchi, K. Tanabe, J. Phys. Chem. 90 (1986) 4194–4196.
[32] T. Luo, R.J. Gorte, Appl. Catal. B: Environ. 53 (2004) 77–85.
[33] P. Bazin, O. Saur, F.C. Meunier, M. Daturi, J.C. Lavalley, A.M. Le Govic, V. Harlé, G. Blanchard, Appl. Catal. B: Environ. 90 (2009) 368–379.
[34] L. Zhang, J. Pierce, V.L. Leung, D. Wang, W.S. Epling, J. Phys. Chem. C 117 (2013) 8282–8289.
[35] S.D. Lin, A.C. Gluhoi, B.E. Nieuwenhuys, Catal. Today 90 (2004) 3–14.
[36] M.C. Kung, H.H. Kung, Catal. Rev. 27 (1985) 425–460.
[37] S.J. Yang, Y.F. Guo, H.Z. Chang, L. Ma, Y. Peng, Z. Qu, N.Q. Yan, C.Z. Wang, J.H. Li, Appl. Catal. B: Environ. 136–137 (2013) 19–28.
[38] M. Ziolek, J. Kujawa, O. Saur, A. Aboulayt, J.C. Lavalley, J. Mol. Catal. A: Chem. 112 (1996) 125–132.
[39] G.Y. Xie, Z.Y. Liu, Z.P. Zhu, Q.Y. Liu, J. Ge, Z.G. Huang, J. Catal. 224 (2004) 42–49.
[40] J.A. Rodriguez, T. Jirsak, A. Freitag, J.C. Hanson, J.Z. Larese, S. Chaturvedi, Catal. Lett. 62 (1999) 113–119.
[41] E. Bêche, P. Charvin, D. Perarnau, S. Abanades, G. Flamant, Surf. Interface Anal. 40 (2008) 264–267.
[42] S. Watanabe, X.L. Ma, C.S. Song, J. Phys. Chem. C 113 (2009) 14249–14257.
[43] M. Boaro, C.d. Leitenburg, G. Dolcetti, A. Trovarelli, M. Graziani, Top. Catal. 16–17 (2001) 229–306.
[44] M.J. Sun, G.J. Zou, S. Xu, X.L. Wang, Mater. Chem. Phys. 134 (2012) 912–920.
[45] W. Mišta, M.A. Małecka, L. Kępiński, Appl. Catal. A: Gen. 368 (2009) 71–78.
[46] K. Smith, J. Mackay, V. Henrich, Phys. Rev. B 35 (1987) 5822–5829.
[47] Y.X. Chen, Y. Jiang, W.Z. Li, R.C. Jin, S.Z. Tang, W.B. Hu, Catal. Today 50 (1999) 39–47.
[48] G. Busca, L. Lietti, G. Ramis, F. Berti, Appl. Catal. B: Environ. 18 (1998) 1–36.
[49] P. Forzatti, Appl. Catal. A: Gen. 222 (2001) 221–236.